8-2006

Chemical diffusion of CO in mixed CO+O adlayers and reaction-front propagation in CO oxidation on Pd(100)

Da-Jiang Liu
Ames Laboratory, dajiang@fi.ameslab.gov

James W. Evans
Iowa State University, evans@ameslab.gov

Chemical diffusion of CO in mixed CO+O adlayers and reaction-front propagation in CO oxidation on Pd(100)

Abstract
Within the framework of a realistic atomistic lattice-gas model, we present the theoretical formulation and simulation procedures for precise analysis of the chemical diffusion flux of highly mobile CO within a nonuniform interacting mixed CO+O adlayer on a Pd(100) surface. The approach applies in both regimes of relatively immobile unequilibrated and fairly mobile near-equilibrated O adlayer distributions. Spatiotemporal behavior in surface reactions is controlled by chemical diffusion in mixed adlayers. Thus, we naturally integrate the above analysis with a previously developed multiscale modeling strategy to describe mesoscale reaction front propagation in CO oxidation on Pd(100). This treatment avoids using a simplified prescription of chemical diffusion and reaction kinetics as in traditional mean-field reaction-diffusion equation approaches.

Keywords
Atomistic lattice-gas model, chemical diffusion flux, reaction-diffusion equation, reaction-front propagation, computer simulation, diffusion in gases, oxidation, palladum, reaction kinetics, surface reactions, carbon monoxide

Comments
The following article appeared in *Journal of Chemical* Physics 125, 5 (2006): 054709 and may be found at doi: 10.1063/1.2221690.

Chemical diffusion of CO in mixed C O + O adlayers and reaction-front propagation in CO oxidation on Pd(100)

Da-Jiang Liu and J. W. Evans

Citation: The Journal of Chemical Physics **125**, 054709 (2006); doi: 10.1063/1.2221690
View online: http://dx.doi.org/10.1063/1.2221690
View Table of Contents: http://scitation.aip.org/content/aip/journal/jcp/125/5?ver=pdfcov
Published by the AIP Publishing

Chemical diffusion of CO in mixed CO+O adlayers and reaction-front propagation in CO oxidation on Pd(100)

Da-Jiang Liu[a)]
Ames Laboratory, U.S. Department of Energy, Ames, Iowa 50011

J. W. Evans
Ames Laboratory, U.S. Department of Energy, Ames, Iowa 50011 and Department of Mathematics, Iowa State University, Ames, Iowa 50011

(Received 3 January 2006; accepted 15 June 2006; published online 2 August 2006)

Within the framework of a realistic atomistic lattice-gas model, we present the theoretical formulation and simulation procedures for precise analysis of the chemical diffusion flux of highly mobile CO within a nonuniform *interacting mixed* CO+O *adlayer* on a Pd(100) surface. The approach applies in both regimes of relatively immobile unequilibrated and fairly mobile near-equilibrated O adlayer distributions. Spatiotemporal behavior in surface reactions is controlled by chemical diffusion in mixed adlayers. Thus, we naturally integrate the above analysis with a previously developed multiscale modeling strategy to describe mesoscale reaction front propagation in CO oxidation on Pd(100). This treatment avoids using a simplified prescription of chemical diffusion and reaction kinetics as in traditional mean-field reaction-diffusion equation approaches. © *2006 American Institute of Physics*. [DOI: 10.1063/1.2221690]

I. INTRODUCTION

Over the past few decades, there have been extensive experimental and theoretical studies of chemical diffusion in dense chemisorbed adlayers on low-index single-crystal metal surfaces. More specifically, these have considered almost exclusively interacting *single-species adlayers*.[1–5] Chemical diffusion controls the transient decay of spatial inhomogeneities in adspecies coverage within such adlayers. Such inhomogeneities are often created "artificially" on the mesoscale of tens to hundreds of microns by laser induced thermal desorption (LITD). For example, LITD can be applied to create a localized "hole" in the adlayer, the filling of which is then monitored by subsequent laser pulses or in real space by photoemission electron microscopy (PEEM). Alternatively, a periodic "adsorbate grating" or coverage modulation can be created by LITD from two interfering laser pulses, the decay of which is monitored using second harmonic generation in reflected light or other techniques. Various scanning microscopy techniques have been used to monitor relaxation of inhomogeneities on shorter length scales. The diffusion coefficient, including any coverage dependence associated with adspecies interactions and ordering, can in principle be extracted from a Boltzmann-Matano analysis of the evolution of the coverage profiles. One caution with these analysis is that the resulting diffusion coefficient may incorporate nonequilibrium effects as well as the influence of surface defects. Finally, we note that much theoretical and simulation analyses of atomistic lattice-gas (LG) models for chemisorbed layers have focused on the behavior of chemical diffusion near phase transition boundaries.

In catalytic reactions on single-crystal metal surfaces, a rich variety of "spontaneous" spatial pattern formation and front propagation can be observed.[5–7] Most observations of these phenomena have been obtained from PEEM (Ref. 5) or low energy electron microscopy.[8] For surface reactions, typically chemical diffusion of highly mobile species such as CO or NO in interacting *mixed reactant adlayers* controls the characteristic length scale of spatial patterns (~microns), the characteristic propagation velocity of reaction fronts (~microns/s),[6] and the detailed structure of the coverage profiles across patterns and fronts (analogous to nonreactive systems).[9] Here, the pattern formation is both spontaneous and persistent (e.g., spiral or other structures for oscillatory or excitable reaction kinetics, and propagating fronts for bistable reaction kinetics),[5,6] rather than being transient as in nonreactive systems. This provides even greater motivation for analysis of the associated chemical diffusion problem.

Despite this fact, there has been little consideration of chemical diffusion in mixed adlayers, which are of relevance to these surface reaction systems. The primary exceptions are some analyses for LG models of ideal mixed adlayers (i.e., noninteracting adlayers except for exclusion of double-site occupancy) where both species are mobile,[10–12] and of stochastic mesoscale mean-field models[13] and simplistic LG models,[14–17] where one species is mobile and the other(s) are immobile. In the latter case, one must effectively consider a percolative-type transport problem. The challenge of extending these previous studies to provide an analysis of chemical diffusion for realistic atomistic LG models of interacting mixed adlayers is the central focus of this paper.

A natural testing ground for analysis of chemical diffusion in surface reaction systems is the CO oxidation reaction on unreconstructed substrates. The Langmuir-Hinshelwood mechanism for this reaction includes the steps $CO(gas) + {}^{*} \leftrightarrow CO(ads)$, $O_2(gas) + 2^{*} \rightarrow 2O(ads)$, and $CO(ads)$

[a)]Electronic mail: dajiang@fi.ameslab.gov

$+O(ads) \rightarrow CO_2(gas)+2^*$, where gas(ads) denotes a gas-phase (adsorbed) species and * denotes an empty surface site.[6,18] Also, CO(ads) is typically highly mobile and O(ads) is relatively immobile. This reaction exhibits bistability at lower temperatures: for a range of CO partial pressure, a reactive steady state (with low CO coverage, θ_{CO}, and high O coverage, θ_O) coexists with inactive steady state (with high θ_{CO} and low θ_O). Both these states are stable, but generally not equally stable, so the more stable can displace the less stable to produce a chemical or trigger wave, i.e., a reaction front. Typically, there is a choice of CO partial pressure (an equistability point) in the "middle" of the bistability region where both states are equally stable, and thus where the reaction front is stationary. Such reaction fronts naturally provide coverage gradients across which we assess the chemical diffusion flux of CO, $\mathbf{J}_{CO}$.

The above front propagation phenomenon can be formally described precisely in terms of *exact* reaction-diffusion equations (RDEs) in the physically relevant hydrodynamic regime corresponding to highly mobile CO(ads).[10] These exact RDEs have the form

$$\partial\theta_{CO}/\partial t = R_{CO}(\theta_{CO},\{O\}) - \nabla\cdot\mathbf{J}_{CO} \quad (1)$$

and

$$\partial\theta_O/\partial t = R_O(\theta_{CO},\{O\}). \quad (2)$$

Here, R_{CO} and R_O describe the adsorption, desorption, and reaction kinetics which generally depend on the entire (possibly unequilibrated) configuration {O} of O(ads), not just on the coverage of locally equilibrated CO(ads) and O(ads). Note that no diffusion flux for relatively immobile O(ads) appears in these hydrodynamic RDEs. Input to these RDEs requires description of both the reaction kinetics and transport properties for generally nonequilibrium nonsteady states distributed across the front.[10,14,19] These states are described below as "front states."

The standard strategy to analyze the above RDEs is to adopt a mean-field form for the reaction kinetics terms (which then just depend on coverages) assuming a "well-stirred" spatially randomized reactant adlayer, and to assume a simple Fick's law expression for $\mathbf{J}_{CO}=-D_{CO}\nabla\theta_{CO}$ with *constant* D_{CO}.[6] Consequently, this treatment ignores interactions and ordering within the reactant adlayer, which impact *both* the reaction kinetics *and* chemical diffusion. An alternative and practical approach potentially allowing precise analysis of the exact RDEs is to implement a *heterogeneous multiscale modeling* strategy.[20] Specifically, using our heterogeneous coupled lattice-gas (HCLG) approach,[10,14,19,21] one can perform parallel simulations of an atomistic lattice-gas model for the reaction, where individual simulations correspond to distinct macroscopic points distributed across the spatial pattern. We simultaneously extract from these simulations a precise characterization of both the local reaction kinetics and transport coefficients for chemical diffusion, and use the latter to suitably couple the parallel simulations to describe mesoscale surface diffusion. This coupling involves periodically redistributing some fraction of the rapidly diffusing particles between adjacent simulation cells in a way consistent with the calculated surface diffusion fluxes (analogous to "method-of-lines" integration of mean-field RDEs).

TABLE I. Lateral interactions between CO and O adsorbates (in eV) as a function of separation d. Strict exclusion of adspecies pairs is implemented for separations $d<a$.

	$d=a$	$d=\sqrt{5}a/2$	$d=\sqrt{2}a$	$d=1.5a$	$d=2a$
CO–CO	0.170	0.097	0.030	0.022	0.000
O–O	0.360	0.206	0.085	0.047	−0.020
CO–O	0.247	0.141	0.050	0.032	0.000

For a more detailed description of this HCLG approach, the reader is referred to previous publications.[14,19,21] The main point of relevance here is that this approach requires as *essential input* a precise calculation of the nontrivial chemical diffusion fluxes in mixed interacting reactant adlayers. The current paper focuses on the procedure for obtaining such fluxes.

In Sec. II, we briefly describe the realistic lattice-gas (LG) model for CO oxidation used in this study. Then, in Sec. III, we present a general theoretical framework and simulation procedure to determine the diffusion flux of CO across a reaction front under conditions where the CO adlayer (but not necessarily the O adlayer) is locally equilibrated. Next, in Sec. IV, we consider the case where the O adlayer is also locally equilibrated, so then a traditional formulation can be implemented describing the CO diffusion flux in terms of coverage gradients via a diffusion tensor (but with off-diagonal components). Some additional comments on the treatment of nonequilibrated adlayers and conclusions are presented in Sec. V.

II. LATTICE-GAS MODEL FOR CO OXIDATION ON Pd(100)

Our analysis will use a general multisite LG model for CO oxidation on unreconstructed metal(100) surfaces, selecting parameters to describe Pd(100). This model is a refinement of one presented previously for CO oxidation on Pd(100),[19,22] and will be discussed further elsewhere. It provides a realistic and flexible description of adlayer structure and dynamics, allowing population of not just the low-coverage adsorption site for each adspecies, but also other sites which might be occupied at higher coverages or under mixed adlayer reaction conditions, or which might correspond to transition states. For the Pd(100) surface, which has a surface lattice constant of $a=2.75$ Å, we consider bridge (br), fourfold hollow (4fh), and top (top) sites. Adsorption site energies for CO(ads) are chosen as 1.60 eV (br), 1.78 eV (4fh), and 2.07 eV (top). For O(ads), 4fh sites have the lowest energy, with br (top) sites being 0.60 eV (1.20 eV) higher. We assume pairwise additive adspecies interactions depending on separation as indicated in Table I. The energy E of any adsorbed molecule is given as the sum of the site binding energy and all adspecies interactions. Our choice of all these energies is guided by density functional theory (DFT) results, but a critical requirement is that selected values recover observed adlayer ordering, detailed features of temperature programed desorption spectra, and heats of adsorption.[19,22] Of some relevance for this study is the fea-

ture that CO(ads) tends to exhibit $c(2\sqrt{2}\times\sqrt{2})R45°$ ordering for CO coverages approaching 0.5 ML (monolayer),[23] and that O(ads) tends to exhibit $p(2\times2)$ ordering for O coverages around 0.25 ML.[24] See also Appendix A and Fig. 4 for illustration of the ordered structures.

The following dynamical processes are included in our reaction model: nonactivated adsorption of CO(gas) on single empty sites of any type at rate P_{CO} (in unit of ML/s); nonactivated dissociative adsorption of O_2(gas) on diagonally adjacent empty 4fh sites, provided that the six adjacent neighbors are free of O(ads) (the eight-site rule[10,14,19,25,26]) at rate P_{O_2} (ML/s); activated desorption of CO with barrier determined by the total adsorption energy (desorption of oxygen is effectively inoperative under typical reaction conditions); reaction to form CO_2(gas) of CO(ads)–O(ads) pairs with a barrier of 0.73 eV (0.95 eV) for pairs separated by a (by $\sqrt{5}a/2$ and $\sqrt{2}a$), where these barriers are based on DFT analysis[27] and comparison with experimental temperature-programed-reaction (TPR) spectra;[28] and diffusive hopping of both CO(ads) and O(ads) as described below.

Our selected diffusion dynamics includes a "short-hop" pathway between br-4fh and br-top pairs with separation $a/2$, and between br-br and 4fh-top pairs with separation $a/\sqrt{2}$. This choice mimics the actual diffusion dynamics better than the conventional choice of hopping just between sites separated by a using either the Metropolis or the initial value approximation method (see below). It thus better captures the local equilibration dynamics, especially at high adsorbate coverages. For each such hop α, we appropriately assign a base rate h_α which equals the physical rate for an isolated adsorbate to hop from the less to the more energetically favored site. In cases where the hop is between adsorbing and transition states (e.g., br-4fh for oxygen), this h_α is set equal to the diffusion prefactor ν chosen with canonical value of 10^{13} s^{-1}. In order to satisfy detailed balance, we then choose the actual hop rate to have the Metropolis form $h=h_\alpha \min[1,\exp(-\beta\Delta E)]$, where $\beta=1/(k_BT)$ and ΔE is the energy change upon hopping.

In practice, we need to cap the h_α by some smaller rate h_0 to avoid the simulations spending prohibitive amount of CPU time attempting to implement diffusion (with high rejection rate). For analysis of local reaction kinetics, this does not create problems, since even a moderate amount of hopping suffices to produce the correct limiting behavior as $h_0 \to h_\alpha$. In this study, h_0 is typically chosen in the range from 10^3 to 10^5 s^{-1}. However, in contrast, reducing h_0 does directly inhibit the associated chemical diffusion flux, so we must scale up results to extract the behavior for the relevant large h_0.

One might also add a conventional "long-hop" pathway for hops between sites of the same type with separation a. Let $h_d=\nu\exp[-\beta E_d]$ denote the effective zero-coverage hop rate, with activation barriers $E_d=0.65$ eV for O(ads) and $E_d=0.24$ eV for CO(ads). Then, for this pathway, the general hop rate is chosen to have a Metropolis form, $h=h_d \min[1,\exp(-\beta\Delta E)]$.[1,3] We include this pathway as an efficient way to produce physically reasonable diffusion fluxes even for small h_0.

Now, we briefly comment further on the utility of our short-hop dynamics for incorporating key physical features of surface diffusion dynamics. It has been demonstrated that the adspecies hop rate may be enhanced (relative to that for an isolated particle) by the presence of repulsive interactions with other adspecies in the initial state.[29] In this case, the interactions increase E for the initial state, but may leave E relatively unchanged for the transition state. Thus, ΔE changes from zero to a negative value for long hops, so the Metropolis hop rate would be unaffected. However, ΔE is reduced from $-E_d$ to a less negative value for hops to a transition state, so the hop rate is enhanced (as desired). Another general feature of our short-hop dynamics is that the hop rate accounts for the effect of adspecies interactions evaluated in the transition state, as is physically appropriate.[30]

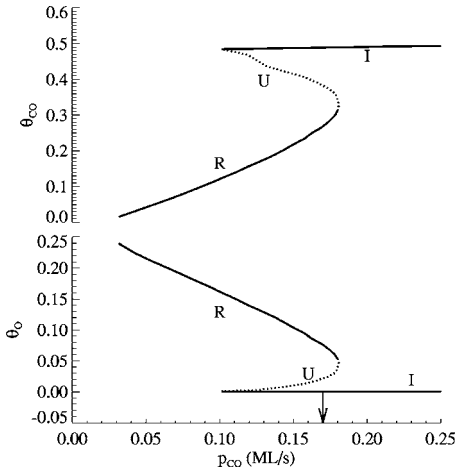

FIG. 1. Steady-state coverage for CO and oxygen for CO oxidation on Pd(100) at $T=380$ K and $P_{O_2}=1$ ML/s. The solid lines represent stable reactive (R) and inactive (I) states, and the connecting dashed lines represent unstable states (U). Also shown by an arrow is the equistability pressure.

Finally, for our subsequent discussion and analysis, it is instructive to illustrate bistability in the steady-state behavior of our reaction model at 380 K. The variation with P_{CO} of the coverages in the reactive and inactive stable steady states and in the unstable steady states (obtained with a constant-coverage simulation algorithm[31]) is shown in Fig. 1.

III. BASIC FORMULATION FOR CO DIFFUSION IN MIXED CO+O ADLAYERS

The conceptual framework needed for determination of chemical diffusion on surfaces is provided by transport theory developed within the broader context of nonequilibrium statistical mechanics. Our treatment will assume that CO(ads) is locally equilibrated in a disordered environment created by coadsorbed relatively immobile O(ads). The detailed arrangement of O(ads) within this disordered environment will be determined by the reaction process and conditions (e.g., partial pressures, temperature, location of the front state under consideration). It will not necessarily be assumed that O(ads) is locally equilibrated. Then, the flux of CO(ads) diffusing across the surface is given in terms of a conductivity Λ_{CO} (making an analogy with electrical conductivity) and a chemical potential μ_{CO}, for CO(ads) by

$$\mathbf{J}_{CO} = -\Lambda_{CO} \nabla \mu_{CO}, \tag{3}$$

where we write

$$\mu_{CO} = \mu_{CO}(\theta_{CO}, \{O\}) \tag{4}$$

and

$$\Lambda_{CO} = \theta_{CO}\sigma_{CO}/(k_B T). \tag{5}$$

We have indicated here that in addition to dependence on θ_{CO}, the chemical potential of CO(ads) generally depends the entire configuration {O} of O(ads) (rather than just θ_O). We have also decomposed the CO conductivity into a product of the "carrier density," θ_{CO}, and a CO mobility, σ_{CO}. The latter can be obtained by analyzing collective many-particle diffusion in a spatially homogeneous $d=2$ dimensional system. Specifically, consider a finite system with periodic boundary conditions which include N_{CO} adsorbed CO with positions $\mathbf{r}_m(t)$, for $1 \leqslant m \leqslant N_{CO}$, calculated so as to vary continuously as particles cross the system boundary (and thus to potentially increase without bound). Then, in terms of the center of mass, $\mathbf{R}_{CO} = \Sigma_m \mathbf{r}_m / N_{CO}$, one has

$$\sigma_{CO} = \lim_{t \gg \tau_{CO}} (2dt)^{-1} |\mathbf{R}_{CO}(t) - \mathbf{R}_{CO}(0)|^2. \tag{6}$$

Here, τ_{CO} is a characteristic time associated with CO hopping. Then, the above limiting behavior should be achieved for times much larger than τ_{CO}, but much shorter than the characteristic time, τ_{react}, associated with adsorption, desorption, and reaction processes (so adspecies coverages in nonequilibrium front states will not have changed significantly over this time scale). Note that the mobility approaches a nonzero constant in the low CO coverage regime, in contrast to the conductivity. The above procedure can be implemented to determine σ_{CO} in each of the simulation cells distributed across the reaction front in a HCLG treatment of front propagation (noting that these have periodic boundary conditions, and that they describe locally spatially homogeneous front states).

The results of such an analysis for the variation of σ_{CO} across a reaction front are shown in Fig. 2, choosing $P_{CO} = 0.17$ ML/s, $P_{O_2} = 1$ ML/s, and $T = 380$ K, which are in the bistability region near the equistability point for 380 K (cf. Fig. 1). The coverage profiles are also shown, so one can correlate behavior of σ_{CO} to that of the coverages. Clearly, σ_{CO} is negligible for the inactive state with high $\theta_{CO} \approx 0.5$ ML, which corresponds to almost perfect $c(2\sqrt{2} \times \sqrt{2})R45°$ CO ordering.[19,22] Also, σ_{CO} increases monotonically scanning across the front from the inactive to reactive state with much lower $\theta_{CO} \approx 0.29$ ML and (still quite low) $\theta_O \approx 0.07$ ML. The value of σ_{CO} in the reactive state is 0.06 times its value in the zero-coverage limit. As an aside, Eq. (6) can be used to analyze the behavior of CO mobility in a broader range of states than those associated with reaction fronts. Such an analysis is presented in Appendix A.

To determine the flux $\mathbf{J}_{CO}$ across the reaction front considered above, it is also necessary to determine the chemical potential μ_{CO} of the locally equilibrated CO adlayer at various points across the front. One convenient procedure which

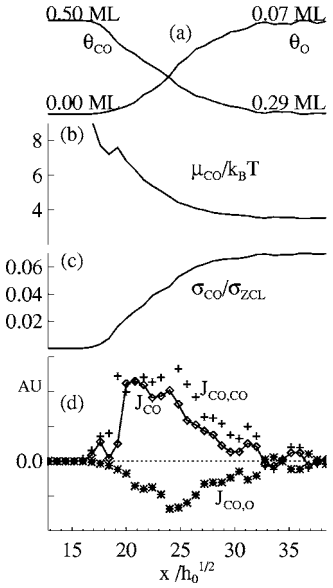

FIG. 2. (a) Coverage profiles; (b) CO chemical potential; (c) CO mobility [normalized by its zero-coverage limit (ZCL)]; and (d) total flux and flux components over a stationary wave front for CO oxidation on Pd(100) with $P_{CO} = 0.17$ ML/s, $P_{O_2} = 1$ ML/s, and $T = 380$ K.

can be employed to obtain μ_{CO} in our simulations is the Widom particle-insertion method.[32] This approach utilizes the formula

$$\mu_{CO}/(k_B T) = \ln \theta_{CO} - \ln[\langle \exp(-\delta E/(k_B T)) \rangle], \tag{7}$$

where δE is the energy cost to insert the particle and $\langle \cdots \rangle$ is an ensemble average. Due to the increased difficulty of insertion as θ_{CO} increases towards 0.5 ML corresponding to a well-ordered CO-$c(2\sqrt{2} \times \sqrt{2})R45°$ state, this procedure becomes less accurate. However, this does not create problems since in this regime, the CO mobility and thus the diffusive flux of CO(ads) are low. Results from this approach for the variation of μ_{CO} across the reaction front are also presented in Fig. 2.

In addition, utilizing the above results for μ_{CO}, we also show in Fig. 2 the behavior of $\mathbf{J}_{CO}$ across the front. CO(ads) diffuses downhill in CO chemical potential, which also corresponds to the downhill direction in CO coverage.

IV. REFINED TREATMENT OF CO DIFFUSION FOR QUASIEQUILIBRATED ADLAYERS

Under typical reaction conditions, O(ads) is also quite mobile, and thus it may be reasonable to assume that the adlayer is completely locally equilibrated (i.e., the local front state corresponds to a Gibbs state with coverages determined by the reaction conditions and the location within the reaction front). In this case, one can apply general transport theory for locally equilibrated n-component surface adlayers, for which the diffusive flux for species i satisfies $\mathbf{J}_i = -\Sigma_{j=1,n} \Lambda_{ij} \nabla \mu_j$, where Λ_{ij} is a so-called conductivity tensor. Significantly, the local chemical potentials μ_j are now determined completely by the coverages $(\theta_1, \ldots, \theta_n)$ and by the surface temperature T. For CO oxidation on metal sur-

faces where i=CO or O, the mobility of CO(ads) far exceeds that of O(ads), so that only $\Lambda_{CO,CO}$ (denoted by Λ_{CO} in Sec. III and below) is significant.

Thus, in contrast to the treatment of Sec. III where we wrote $\mu_{CO}=\mu_{CO}(\theta_{CO},\{O\})$ depending on the entire configuration $\{O\}$ of the possibly unequilibrated O adlayer, here we have $\mu_{CO}=\mu_{CO}(\theta_{CO},\theta_O)$ (leaving implicit the dependence on T). It then follows that

$$\nabla\mu_{CO}=\partial\mu_{CO}/\partial\theta_{CO}\,\nabla\,\theta_{CO}+\partial\mu_{CO}/\partial\theta_O\,\nabla\,\theta_O, \tag{8}$$

so

$$\mathbf{J}_{CO}=-D_{CO,CO}\,\nabla\,\theta_{CO}-D_{CO,O}\,\nabla\,\theta_O, \tag{9}$$

where $D_{CO,j}=\Lambda_{CO}\partial\mu_{CO}/\partial\theta_j$ and below we set $\mathbf{J}_{CO,j}=-D_{CO,j}\nabla\,\theta_j$.

In a conventional treatment for locally equilibrated n-component systems, one writes $\nabla\theta_i=\Sigma_j\chi_{i,j}\nabla\mu_j$, where $\chi_{i,j}=\partial\theta_i/\partial\mu_j$ are the components of a compressibility tensor. A simple calculation utilizing the equilibrium grand canonical partition function reveals that the latter quantity can be reexpressed as $\chi_{i,j}=(k_BT)^{-1}V\langle\delta\theta_i\delta\theta_j\rangle$, where $\delta\theta_i=\theta_i-\langle\theta_i\rangle$ describes the deviation of the coverage from its mean value. Here, V denotes the size (in units of a^2) of the subsystem over which the fluctuations are quantified in terms of a temporal average, $\langle\ldots\rangle$. For our application, one should choose $V\gg1$, but the linear size of this region should be significantly smaller than the characteristic length associated with CO diffusion. Also, the temporal average should be taken over times far shorter than the characteristic time τ_{react} associated with adsorption, desorption, and reaction, and far exceeding the time τ_{CO} associated with CO hopping, just as for the evaluation of σ_{CO}. However, now this average should also extend over times far exceeding the characteristic time τ_O associated with O hopping. In this way, the fluctuations will correctly reflect the completely locally equilibrated state associated with both adspecies diffusing into and out of the subsystem (see Appendix B). Finally, using the identity $\partial\mu_i/\partial\theta_j=(\chi^{-1})_{i,j}$, one can recast expressions for the components of the diffusion tensor in Eq. (9) in terms of the components of the conductivity and compressibility tensors.[33]

In our application where CO mobility dominates O mobility, there are just two non-negligible diffusion coefficients

$$D_{CO,CO}=\frac{\Lambda_{CO}}{\chi_{CO,CO}-\chi_{CO,O}^2\chi_{O,O}^{-1}} \tag{10}$$

and

$$D_{CO,O}=-\chi_{CO,O}\chi_{O,O}^{-1}D_{CO,CO}. \tag{11}$$

In the low-coverage noninteracting regime, one has $\chi_{i,i}\propto\theta_i(1-\theta_i)$ and $\chi_{i,j}\propto-\theta_i\theta_j$ for $i\neq j$, so $D_{CO,O}\approx\theta_{CO}/(1-\theta_O)D_{CO,CO}$. The latter relationship applies exactly for all coverages in idealized models where CO–CO and CO–O interactions are ignored.[10,11,14,15,17] To summarize, as is the case for single-component interacting systems, evaluation of the diffusion coefficients requires determination of both kinetic components (conductivities or mobilities) and thermodynamic components (compressibilities or fluctuations).

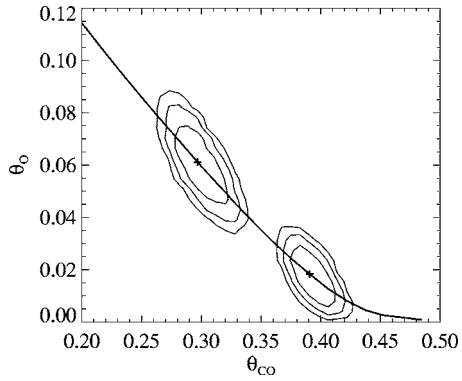

FIG. 3. 2D contour plots indicating coverage distributions choosing $V=256$ for two selected front states with mean coverages $(\theta_{CO},\theta_O)=(0.297,0.061)$ and (0.391, 0.018). Also shown is the continuous locus of mean coverages across front.

Determination of the CO conductivity or mobility was described above in Sec. III. Thus, here we focus on analysis of coverage fluctuations in the front states. It is instructive to examine the full coverage distribution for the front states determined within a finite subregion region of size V under conditions described above. Noting that the width of the distribution scales like $V^{-1/2}$, typical results for $V=256$ lattice sites are shown in Fig. 3 for two separate front states. These results indicate a Gaussian-type distribution with distortion reflecting a negative correlation between fluctuations in the CO and O coverages, $\chi_{CO,O}<0$, i.e., the contours of equal probability have a roughly elliptical shape with the semimajor axis having a negative slope in the (θ_{CO},θ_O) plane (see Appendix B). In representing this distribution, we indicate that the peak corresponds to the mean coverage for the associated front state by also including in the plot the curve indicating the locus of the mean CO and O coverages across the front.

From the full coverage distribution, one can readily extract the $\chi_{i,j}$ needed to determine $D_{CO,CO}$ and $D_{CO,O}$. Results for the corresponding components of the total CO-diffusive flux $\mathbf{J}_{CO}$ are also shown in Fig. 2. Note that since $\chi_{CO,O}<0$, as indicated above, one has that $D_{CO,O}>0$ (as well as $D_{CO,CO}>0$). Thus, $\mathbf{J}_{CO,CO}=-D_{CO,CO}\nabla\,\theta_{CO}$ is downhill in the CO-coverage gradient (i.e., to the right in Fig. 2), and $\mathbf{J}_{CO,O}=-D_{CO,O}\nabla\,\theta_O$ is downhill in the O-coverage gradient (i.e., in the opposite direction, to the left in Fig. 2). Together these two fluxes sum to roughly equal the total flux $\mathbf{J}_{CO}$ calculated in Sec. III (noting that there is necessarily significant statistical uncertainty in our simulation data, and also that the adlayer may not be fully equilibrated).

V. FURTHER DISCUSSION AND CONCLUSIONS

The formulation in Sec. IV assumes complete local equilibration of the adlayer. Often, this condition is also required in multiscale simulation procedures,[20,34] where the microscopic state must be reconstructed from a few macrovariables (but this is not the case for our HCLG approach [14,19]). While local equilibration is typically satisfied for the CO adlayer, there are some situations where this condition

may not be met for the O adlayer. It is instructive to elaborate on such cases, noting that one can still apply the general formulation of Sec. III.

For sufficiently low T, limited O mobility will inhibit equilibration of the O adlayer,[26] and will not be possible to characterize these states in terms of a few macrovariables. However, since the typical reaction barrier for CO oxidation on Pd(100) of ~1 eV is significantly above the low-coverage O(ads) diffusion barrier of ~0.6 eV, one should expect O mobility to be significant under typical reaction conditions. Another more subtle source of the lack of equilibration arises for propagating fronts with low P_{CO}, where a reactive state with high θ_O displaces an inactive state. Here, one expects symmetry breaking of the O adlayer in the reactive steady state[10,14,35] [e.g., a transition to $p(2\times2)$ long-range order when θ_O increases above ~0.25 ML]. Then, as the reaction front passes by, the O coverage will increase and exceed the critical value for symmetry breaking in the steady state. However, symmetry cannot be broken globally in the finite time since the front has passed, so the front states will be composed of collections of finite symmetry-broken domains in various states of coarsening. This degree of coarsening may significantly impact the transport coefficients especially if CO diffusion occurs preferentially along domain boundaries.[14]

Another complication arises from the feature that the CO adlayer can exhibit a first-order transition from disorder to long-range $c(2\sqrt{2}\times\sqrt{2})R45^\circ$ order for θ_{CO} close to 0.5 ML. This will also impact detailed front structure. In a separate work, we will discuss refinement of the above formulation to address various nonequilibrium situations.

In summary, we have presented a formulation and techniques allowing the analysis of a new class of chemical diffusion problems involving realistic atomistic LG models for interacting mixed adlayers relevant for CO oxidation systems. This analysis and the resulting characterization of diffusivity are key components to the description of reaction fronts in such surface reactions.

ACKNOWLEDGMENTS

This work was supported by the Division of Chemical Sciences and by the SciDAC Computational Chemistry program of the U.S. Department of Energy (Basic Energy Sciences). It was performed at Ames Laboratory which is operated for the USDOE by Iowa State University under Contract No. W-7405-Eng-82.

APPENDIX A: FURTHER CHARACTERIZATION OF THE BEHAVIOR OF CO MOBILITY

The procedure described in Sec. III for the analysis of CO mobility σ_{CO} can be applied to a wider class of states than those associated with reaction fronts. Indeed, it is instructive to assess how σ_{CO} varies over a broader range of adlayer coverages and ordering. (The same applies for the analysis of coverage fluctuations or the compressibility tensor.) It is particularly natural to analyze the behavior of σ_{CO} in the steady states of the reaction model, e.g., at constant T and P_{O_2} for varying P_{CO}. Significantly, this is possible not just for stable steady states, but also for unstable steady states (utilizing a constant-coverage simulation algorithm[31]), thus allowing characterization for a continuous broad range of coverage.

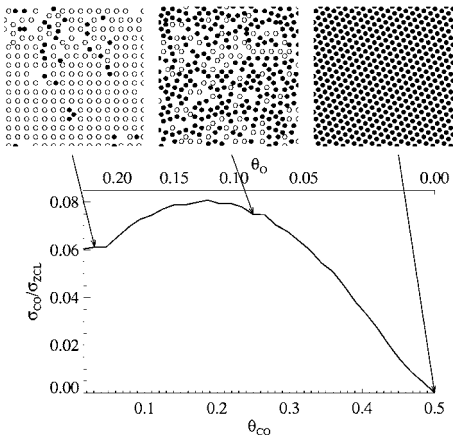

FIG. 4. CO mobility (normalized by the zero-coverage limit) of the steady states for CO oxidation on Pd(100) at $T=380$ K and $P_{O_2}=1$ ML/s. Shown above are snapshots of the adsorbate configurations under different conditions, with CO(ads) denoted by black circles and O(ads) by open circles. Well-defined CO-$c(2\sqrt{2}\times\sqrt{2})R45^\circ$ ordering is shown on the right for $\theta_{CO}\approx0.5$ ML, and regions of well-defined O-$p(2\times2)$ ordering are shown on the left.

Results from such an analysis choosing $T=380$ K and $P_{O_2}=1$ ML/s (i.e., for the steady states corresponding to Fig. 1) are presented in Fig. 4. As for the front states, σ_{CO} is negligible for states with high $\theta_{CO}\sim0.5$ ML and near-perfect CO-$c(2\sqrt{2}\times\sqrt{2})R45^\circ$ ordering. Also, σ_{CO} increases with decreasing θ_{CO}. However, it achieves a maximum around $\theta_{CO}\sim0.2$ ML, and decreases for lower θ_{CO} and higher θ_O. This is because the high coverage of O(ads) close to 0.25 ML and well-defined O-$p(2\times2)$ ordering inhibit mobility of CO(ads), which must "percolate" through the coadsorbate.

APPENDIX B: TIME AND LENGTH SCALES IN ANALYSIS OF COVERAGE FLUCTUATIONS

We have noted in Sec. IV that for analysis of coverage fluctuations, it is necessary to average over time scales larger than both τ_{CO} and τ_O (and shorter than τ_{react}). This allows both CO and O adspecies to diffuse into and out of the subsystem of finite size V under consideration. Alternatively, one could average over shorter times $\tau_{CO}\ll t\ll\tau_O$, but then θ_O is essentially fixed for a single subsystem, so one must sample over many subsystems to correctly recover the distribution of θ_O. [Note that for the analysis of σ_{CO}, it typically suffices to average over shorter times $\tau_{CO}\ll t\ll\tau_O$ since the diffusing CO(ads) will still sample over many local configurations of O(ads).] Finally, we should note that the negative correlation between CO and O coverage fluctuations might be expected, in general, for coadsorbate systems based on general fluctuation-correlation relations.[36]

Some previous analyses of fluctuations have considered the behavior in reaction systems of strictly finite size V (rather than just in finite subsystems) and for time scales longer than τ_{react}.[36–38] In this regime, fluctuations are controlled by the adsorption, desorption, and reaction processes

(rather than by diffusion processes), and different phenomena emerge such as critical fluctuations near cusp points associated with the loss of bistability. However, in our studies of diffusion, fluctuations are measured in a small subsystem contained within a much larger system (with linear size bounded above by the CO-diffusion length). For this large system, as well as for small subsystems contained within, fluctuations associated with adsorption, desorption, and reaction are quenched by rapid CO diffusion. Thus, critical fluctuations are not relevant for exact RDEs in the hydrodynamic limit.

APPENDIX C: SPECIAL PROCEDURES FOR STATIONARY FRONTS

In our general HCLG multiscale modeling description of spatial pattern formation or reaction front propagation in surface reaction-diffusion systems, it is necessary to simultaneously simulate the state of various macroscopic points distributed across the pattern or front and to implement suitable coupling reflecting surface diffusion.[14,19,21] However, for the special case of stationary reaction fronts at equistability, we show here that it is possible to decouple these simulations, i.e., to perform them one at a time, and then to reconstruct the front profile utilizing data from the individual simulations.

This possibility exploits a special feature of front states at equistability corresponding to a CO partial pressure of $P_{CO}=P_{CO}^{eq}$, say, for fixed P_{O_2}: these states are completely equivalent to steady states of the reaction model for this same P_{O_2}, but with varying P_{CO}. These steady states could be either stable or unstable depending on the coverages. This equivalence of states can be readily anticipated from Eq. (2) as this same equation setting $\partial\theta_O=0$ applies to both steady states and front states for the same fixed P_{O_2}. This would not be the case in a model with significant chemical diffusion of O(ads) in the hydrodynamic regime. Then Eq. (2) would include an extra term involving the diffusion flux for O(ads) which would vanish for homogeneous steady states, but not for front states. It is also clear from Eq. (2) that front states in propagating waves are distinct from any steady states.

In explaining our strategy for performing decoupled simulations, we note that for front states at equistability, the left-hand side of Eq. (1) also vanishes. Furthermore, this is accomplished by a balance between the kinetic term and the diffusive flux term on the right-hand side, i.e.,

$$-R_{CO}=-\nabla\cdot\mathbf{J}_{CO}. \tag{C1}$$

Thus, in our decoupled simulations, we use a modified constant-coverage-type algorithm, where we fix the CO coverage and O_2 pressure and monitor the CO "addition rate" required to maintain the fixed CO coverage. If the coverage of CO drops below a certain target (due to desorption or reaction), attempts are made to deposit CO on the surface. The rate for such *attempts* corresponds to an effective CO pressure, P_{eff}, which generally differs from the physical pressure P_{CO}^{eq} at equistability. The role of the diffusional flux described above for front states is played by an extra inflow or outflow of CO corresponding to nonzero values of $\delta P=P_{eff}-P_{CO}^{eq}$. Based on the above remarks, we claim that the states generated from these constant-coverage simulations are statistically equivalent to the stationary front states obtained by parallel simulations with the same CO coverage (for rapid CO diffusion). Consequently, the former can be used to assess reaction kinetics and transport properties.

The above analysis suffices to obtain the reaction kinetics or transport properties across the front as functions of either the CO or O coverage. However, to reconstruct the spatial coverage profile across the front using data from the constant-coverage simulations requires the following additional steps. First, from the constant-coverage simulations, we must also extract a normalized sticking coefficient, $S_{CO}(\theta_{CO},\{O\})$, for CO which measures the success probability of adsorption per attempt. Then, since the excess CO flux in the constant coverage simulations, $(P_{eff}-P_{CO}^{eq})S_{CO}$ corresponds to the diffusive flux in Eq. (C1), it follows that

$$R_{CO}(\theta_{CO},\{O\})=-(P_{eff}-P_{CO}^{eq})S_{CO}(\theta_{CO},\{O\}). \tag{C2}$$

In this way, we obtain R_{CO} for front states as both P_{eff} and S_{CO} can be measured directly from simulations. Since we now know the variation with θ_{CO} of the kinetics term R_{CO} across the front (as well as the variation of various other quantities such as Λ_{CO}, μ_{CO}, $D_{CO,CO}$, $D_{CO,O}$, and θ_O), we can recast Eq. (C1) as

$$\frac{\partial}{\partial x}\left[D_{CO}^{eff}(\theta_{CO})\frac{\partial}{\partial x}\theta_{CO}\right]=R_{CO}(\theta_{CO}), \tag{C3}$$

with

$$D_{CO}^{eff}=\Lambda_{CO}\frac{d\mu_{CO}}{d\theta_{CO}}=D_{CO,CO}(\theta_{CO})+D_{CO,O}(\theta_{CO})\frac{d\theta_O}{d\theta_{CO}}. \tag{C4}$$

In the last equation, $d/d\theta_{CO}$ should be regarded as a total derivative along the front states. The profile can be obtained by integrating this second-order ODE using either a shooting method or a relaxation method.

[1] R. Gomer, Rep. Prog. Phys. **53**, 917 (1990).
[2] *Surface Diffusion: Atomistic and Collective Processes*, NATO Advanced Studies Institute, Series B: Physics Vol. 360, edited by M. C. Tringides (Plenum, New York, 1996).
[3] T. Ala-Nissila, R. Ferrando, and S. C. Ying, Adv. Phys. **51**, 949 (2002).
[4] *Surface Mobilities on Solid Materials: Fundamental Concepts and Applications*, NATO Advanced Studies Institute Series B: Physics Vol 86, edited by V. Thien Binh (Plenum, New York, 1983).
[5] H. H. Rotermund, Surf. Sci. Rep. **29**, 265 (1997).
[6] R. Imbihl and G. Ertl, Chem. Rev. (Washington, D.C.) **95**, 697 (1995).
[7] M. Eiswirth and G. Ertl, in *Chemical Waves and Patterns*, edited by R. Kapral and K. Showalter (Kluwer, Dordrecht, 1995), pp. 447–484.
[8] K. C. Rose, D. Battogtokh, A. Mikhailov, R. Imbihl, W. Engel, and A. M. Bradshaw, Phys. Rev. Lett. **76**, 3582 (1996).
[9] W. Swiech, C. S. Rastomjee, R. Imbihl, J. W. Evans, B. Rausenberger, W. Engel, A. K. Schmid, A. M. Bradshaw, and E. Zeitler, Surf. Sci. **307**, 138 (1994).
[10] J. W. Evans, D.-J. Liu, and M. Tammaro, Chaos **12**, 131 (2002).
[11] V. P. Zhdanov, Surf. Sci. **194**, 1 (1988).
[12] K. W. Kehr, K. Binder, and S. M. Reulein, Phys. Rev. B **39**, 4891 (1989).
[13] M. Hildebrand, Chaos **12**, 144 (2002).
[14] D.-J. Liu and J. W. Evans, Multiscale Model. Simul. **4**, 424 (2005).
[15] M. Tammaro and J. W. Evans, J. Chem. Phys. **108**, 762 (1998).
[16] M. Tammaro and J. W. Evans, J. Chem. Phys. **108**, 7795 (1998).
[17] D.-J. Liu and J. W. Evans, J. Chem. Phys. **113**, 10252 (2000).

[18] R. Imbihl, Prog. Surf. Sci. **44**, 185 (1993).
[19] D.-J. Liu and J. W. Evans, Phys. Rev. B **70**, 193408 (2004).
[20] W. E and B. Engquist, Commun. Math. Sci. **1**, 87 (2003).
[21] M. Tammaro, M. Sabella, and J. W. Evans, J. Chem. Phys. **103**, 10277 (1995).
[22] D.-J. Liu and J. W. Evans, J. Chem. Phys. **124**, 154705 (2006).
[23] R. J. Behm, K. Christmann, G. Ertl, and M. A. Van Hove, J. Chem. Phys. **73**, 2984 (1980).
[24] S.-L. Chang and P. A. Thiel, J. Chem. Phys. **88**, 2071 (1988).
[25] C. R. Brundle, R. J. Behm, and J. A. Barker, J. Vac. Sci. Technol. A **2**, 1038 (1984).
[26] S.-L. Chang and P. A. Thiel, Phys. Rev. Lett. **59**, 296 (1987).
[27] C. J. Zhang and P. Hu, J. Am. Chem. Soc. **123**, 1166 (2001).
[28] E. M. Stuve, R. J. Madix, and C. R. Brundle, Surf. Sci. **146**, 155 (1984).
[29] S. Renisch, R. Schuster, J. Wintterlin, and G. Ertl, Phys. Rev. Lett. **82**, 3839 (1999).
[30] V. P. Zhdanov, *Elementary Physicochemical Processes on Solid Surfaces* (Plenum, New York, 1991).
[31] R. M. Ziff and B. J. Brosilow, Phys. Rev. A **46**, 4630 (1992).
[32] B. Widom, J. Chem. Phys. **39**, 2808 (1963).
[33] For a general locally equilibrated multicomponent system, the diffusion tensor satisfies $D=\Lambda\cdot\chi^{-1}$.
[34] C. W. Gear, J. Li, and I. G. Kevrekidis, Phys. Lett. A **316**, 190 (2003).
[35] D.-J. Liu and J. W. Evans, Phys. Rev. Lett. **84**, 955 (2000).
[36] Y. Suchorski, J. Beben, R. Imbihl, E. W. James, D.-J. Liu, and J. W. Evans, Phys. Rev. B **63**, 165417 (2001).
[37] Y. Suchorski, J. Beben, E. W. James, J. W. Evans, and R. Imbihl, Phys. Rev. Lett. **82**, 1907 (1999).
[38] D.-J. Liu, N. Pavlenko, and J. W. Evans, J. Stat. Phys. **114**, 101 (2004).